International Journal of Bifurcation and Chaos

IN-DEPTH ANALYSIS OF SMOOTH AND NONSMOOTH BIFURCATIONS FOR AN OPEN-LOOP BOOST CONVERTER FEEDING CONSTANT POWER LOADS IN DISCONTINUOUS CONDUCTION MODE

LUIS BENADERO
Universitat Politecnica de Catalunya
Barcelona, SPAIN
luis.benadero@upc.edu

ABDELALI EL AROUDI*
Universitat Rovira i Virgili
Tarragona, SPAIN
abdelali.elaroudi@urv.cat

LUIS MARTINEZ-SALAMERO
Universitat Rovira i Virgili
Tarragona, SPAIN
luis.martinez@urv.cat

Chi K. TSE
City University of Hong Kong
Kowloon Tong, Hong Kong
michael.tse@cityu.edu.hk

Received (to be inserted by publisher)

This paper presents a study of the existence conditions of limit cycles and mechanisms of losing their stability for an open-loop DC-DC boost converter loaded with a constant power load and operating in discontinuous conduction mode. First, the existence conditions are determined. Then, boundaries associated with different kinds of instabilities such as the classical smooth fold and period-doubling bifurcations and nonsmooth border-collision bifurcations such as fold border-collision bifurcations are elucidated. To perform the stability analysis, an implicit 1D map for the system is derived. From this model, it is obtained that smooth period-doubling and fold bifurcations may occur at certain values of the circuit parameters. Some results from numerical simulations performed on the circuit-based switched model are provided showing consistency with the theoretical analysis from the derived model.

Keywords: Bifurcation, open-loop, power converter, limit cycle, stability analysis.

*Corresponding author.

1. Introduction

Switching power converters are widely used in different industrial applications such as in portable devices, solid-state lighting drivers and technologies [Leng et al., 2018], electric vehicles, aircraft and ships [Griffo & Wang, 2012; Rivetta et al., 2004; Rahimi & Emadi, 2009; Sulligoi et al., 2014], renewable energy production such as in PV systems [Kwasinski & Onwuchekwa, 2011; Al-Nussairi et al., 2017], among others. Apart from inductive and capacitive energy storage elements, elementary switching converters use two basic switching devices for their operation: a controlled switch (transistor S) and an uncontrolled one (diode D). Depending on the minimum value of the inductor current in each switching period, switching converters operation can be divided into two different modes. If the controlled switch is turned ON before the inductor is completely discharged, then the inductor current never drops to zero and this operation is called continuous conduction mode (CCM). In this operation mode, the state of the controlled switch S and the uncontrolled one D are complementary to each other, i.e., when S is ON D is OFF and vice versa. Alternately, if the inductor is completely discharged before a new switching period starts, then there is a time interval during which the inductor current is zero because both S and D are OFF, and the converter is said to operate in discontinuous conduction mode (DCM) [Tse & Adams, 1990]. In most of the applications, CCM is employed. Yet, DCM can also be used for certain applications such as in power factor correction [Wu et al., 2006]. Moreover, even for applications where CCM is desired, power converters may inevitably enter into DCM operation under some circumstances. For instance in photovoltaic systems, during the early mornings or the late afternoons, when the solar irradiance level is low, the power converter interface may operate in DCM [Bharadwaj & John, 2014].

In new and emerging applications of energy conversion systems and technologies, single-stage power converters fail to meet some of the requirements. Consequently, the two-stage approach with individually regulated converters is used. In a two-stage system an upstream switching converter is driving one or more downstream converters. The downstream converters in a two-stage system are designed to provide the fastest transient response in stand-alone operation. Consequently, in average and within their control bandwidth, they behave as a constant power load (CPL) to the upstream converter [Belkhayat et al., 1995; Chu et al., 2009].

The desired steady-state regime of a power converter is a limit cycle with the same period as an external driving signal [van der Woude et al., 2002]. However, due to their switching nonlinearity and feedback loops, these systems are very rich in nonlinear dynamics [Deane & Hamill, 1990; Banerjee & Verghese, 2001; Tse, 2003; Hamill, 1995]. The common denominator in all the past studies in this research field is the consideration of a closed loop converter either under voltage mode control [Chakrabarty et al., 1996; Fossas & Olivar, 1996; Papafotiou & Margaris, 2004; Tse, 1994-a,b; El Aroudi et al., 2001; Giaouris et al., 2008; Cheng et al., 2017] or current mode control [Redl & Novak, 1981; Zafrany & Ben-Yaakov, 1995; Kabe et al., 2007] and considering a linear, either resistive [Chakrabarty et al., 1996; Fossas & Olivar, 1996; Papafotiou & Margaris, 2004; Tse, 1994-a,b; El Aroudi et al., 2001; Giaouris et al., 2008], constant voltage [Kabe et al., 2007] or constant current load [Cheng et al., 2017]. For these cases, the piecewise linear state equations are employed to obtain the 1D map and the stability analysis of limit cycles passes through solving the eigenvalues problem of the Jacobian matrix of this model. This approach has been widely used for analyzing different kind of switching converters under different control strategies in most of the previous references.

Fast-scale instabilities such as classical smooth period-doubling and fold bifurcations [Tse & Li, 2011; El Aroudi et al., 2005; Wolf et al., 1994; Chen et al., 2008; Giaouris et al., 2009; Mandal & Banerjee, 2015; Cortes et al., 2015], and nonsmooth border-collision bifurcations such as border-collision fold, pitchfork and period-doubling bifurcations [Banerjee et al., 2000; Robert & Robert, 2002; Avrutin & Zhusubaliyev, 2020; Zhang et al., 2022; Gain & Banerjee, 2003; di Bernardo et al., 2001] cannot be predicted by conventional averaged models and has been widely addressed for power converters with linear resistive loads [Chen et al., 2008; Giaouris et al., 2009]. With a linear load, the switched model of a DC-DC converter is piecewise affine and discrete-time modeling and Floquet theory can be straightforwardly applied to predict its fast-scale behavior [Giaouris et al., 2009; Mandal & Banerjee, 2015; Cortes et al., 2015]. Much less efforts have been made to model DC-DC converters operating in DCM for which the inductor current does not contribute to

the system discrete time dynamics. The analysis of fast-scale dynamics of switching converters operating in DCM is generally more complex because DCM has three sub-intervals in a switching cycle. In [Tse, 1994-a,b], discrete-time 1D maps for the boost and the buck converter operating in DCM with a resistive load and under voltage mode control were derived using a finite series approximation of the state transition matrices of the linear equations describing the dynamics of the converter during each switching sub-interval. Using these models, it was shown that voltage mode controlled buck and boost converters with a resistive load operating in DCM exhibit typical period-doubling route to chaos.

Instabilities in switching converters loaded by CPLs have been a topic of extensive research during the recent years in different industrial applications such as in automotive systems [Emadi et al., 2006; Rahimi & Emadi, 2009], microgrids [Onwuchekwa & Kwasinski, 2010], electrified transportation [Gavagsaz-Ghoachani et al., 2013; Saublet et al., 2016-a,b; Gavagsaz-Ghoachani et al., 2017; Zadeh et al., 2016], and power factor correction [Chu et al., 2009] among others. The model of a switching converter with a CPL is nonlinear for each switch state and its discrete-time model describing its dynamical behavior from a switching cycle to the next one cannot be analytically derived. That is why the analysis of the dynamics of switching converters loaded by other converters or other devices acting as CPLs has been widely addressed using conventional averaged models. The small-signal stability issues at the low-frequency slow-scale are often tackled by employing Middlebrook's impedance criterion in the same way when input filter design is addressed [Middlebrook, 1976]. Most of the studies have focused on low frequency behavior using averaged models which gives accurate results only when the natural frequencies of the converter are enough smaller than the switching frequency [Chu et al., 2009; Benadero et al., 2015; Cristiano et al., 2016]. In [Rahimi & Emadi, 2010] using a conventional averaged model it has been claimed that open-loop DC-DC converters operating in DCM are stable when they are loaded by CPLs. Complex numerically obtained discrete-time models or improved averaged models have been used for more accurate prediction of instabilities [Gavagsaz-Ghoachani et al., 2017; Saublet et al., 2016-a,b; Zadeh et al., 2016]. With a nonlinear load such as a CPL, DC-DC converters may exhibit fast-scale instability not only in closed loop [El Aroudi et al., 2019] but also in open loop [Benadero et al., 2020].

It is worth to note that the CPL model of the load converter can be made more realistic by taking into account bandwidth limitation and ripple in its state variables. Often, simplifications and approximations based on realistic assumptions are used to obtain simplified models that allow a profound understanding of the system behavior. Good matching between the model and the actual system can be obtained even under doing these approximations. The usual idealization of the downstream converter is to consider it as a CPL leading naturally to a static equation for this stage hence to a significant order-reduction of the source converter model. The effect of the different parameters of the source converter from the perspective of its stability can be therefore revealed using reduced-order models. Another way to deal with the stability analysis of cascaded converters without considering the load converter as a CPL is by performing this analysis on the complete system [Zhang et al., 2023], [El Aroudi et al., 2016]. In this case some peculiar effects such as the impact of the ripple of the state variables of the downstream converter on the upstream converter stability can be revealed [Zhang et al., 2023], [El Aroudi et al., 2016]. In particular in [Zhang et al., 2023] it has been shown by theoretical analysis, numerical simulations and experimental results that the input current ripple of a downstream buck converter can change the stability of an upstream buck converter. In [El Aroudi et al., 2016] it was shown that stability range of a current mode controlled upstream boost converter can be enlarged by the ripple of the intermediate capacitor voltage revealing a stabilizing effect of this ripple. The results have been obtained first by a full-order model and also by a reduced order model where the current mode controlled downstream boost converter has been approximated by its steady-state model represented by a current sink. The matching between the results obtained from both models was remarkable.

Following our previous work in [Benadero et al., 2020], the aim of this paper is to present an in-depth study of the mechanisms of losing the stability of a DC-DC boost converter loaded with a CPL and operating in DCM. Existence conditions of limit cycles are determined and an analysis of their possible bifurcation is performed showing that the converter can exhibit both classical smooth period-doubling and fold bifurcations and some nonsmooth border collision bifurcations. The conditions leading to these bifurcations are deduced and their boundaries are located in a normalized parameter space. With a nonlinear load such

as a CPL, the discrete-time map can only be obtained implicitly. However, under some assumptions to be detailed later an explicit 1D map will be derived. The effect of the different system parameters from the perspective of system stability is revealed. The approach used shows its effectiveness in instability analysis of power converters working in DCM with nonlinear loads such as a CPL.

The rest of this paper is organized as follows: after this introduction, in Section 2 the description and the switched model of the system under study are presented. The nonlinear dynamic behavior is addressed in Section 3 where existence conditions, stability analysis and bifurcation analysis of limit cycles are addressed. Finally, Section 4 summarizes the conclusions of this work.

2. Circuit scheme and normalized switched model

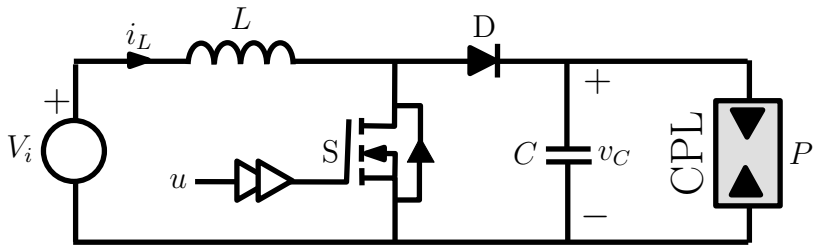

Fig. 1. Schematic circuit diagram of an open-loop DC-DC boost converter loaded with a CPL.

The circuit schematic diagram of an open loop DC-DC boost converter is shown in Fig. 1. The energy is supplied by a voltage source V_i and drained into the load, which is assumed to be a CPL with a power P. The state variables of the system are v_C and i_L, that is the voltage across the capacitor, with capacitance C, and the current through the inductor, with inductance L. The switch S is driven by a periodic square-wave signal $u(t)$ with switching period T_s and duty ratio D, such that within an entire switching cycle, one has $u = 1$ thus turning ON the switch S during the time sub-interval from nT_s ($n \in \mathbb{N}$) to $(n + D)T_s$, and $u = 0$ during the rest of the cycle until $(n + 1)T_s$, and so the switch S is turned OFF. From voltage and current Kirchhoff's laws, the corresponding state equations are

$$\begin{aligned} \frac{dv_C}{dt} &= -\frac{P}{Cv_C} + \frac{(1-u)i_L}{C} \\ \frac{di_L}{dt} &= \frac{(u-1)v_C}{L} + \frac{V_i}{L} \end{aligned}, \tag{1}$$

where $u = 1$ and $u = 0$ during the ON and the OFF intervals respectively. In order to reduce the number of parameters of the system and to simplify the analysis, let us define the dimensionless time (τ), the state variables (x, y) and the parameters (p, T) as follows

$$\tau = \omega_0 t, \quad x = \frac{v_C}{V_i}, \quad y = \frac{Z_0 i_L}{V_i}, \quad p = \frac{PZ_0}{V_i^2}, \quad T = \omega_0 T_s,$$

where ω_0 is the natural frequency and Z_0 is the characteristic impedance of the LC circuit. These are given by

$$\omega_0 = \frac{1}{\sqrt{LC}}, \quad Z_0 = \sqrt{\frac{L}{C}}.$$

Then, with a slight abuse of notation taking t instead of τ as the normalized time, the differential system (1) becomes

$$\begin{aligned} \frac{dx}{dt} &= -\frac{p}{x} + (1-u)y \\ \frac{dy}{dt} &= (u-1)x + 1 \end{aligned}. \tag{2}$$

System (2) has an unstable equilibrium for the OFF topology ($u = 0$) at the point $X^*_{off} = (1, p)$. Note that for this topology, one has $dy/dt = 1 - x$, and assuming $y \geq 0$, the OFF trajectory points to abscissa if $x > 1$, leaves from it if $x < 1$ and it is tangent at the critical point $(1, 0)$, because at this point one has $dy/dt = 0$. This fact implies a visible tangency [Jefferies, 2009] at the point $(1, 0)$.

The DCM condition takes place if the inductor current becomes null during the OFF interval, at a point $(x, 0)$ (being $x > 1$), thus defining a third time interval during which the two switches (transistor and diode) are OFF and it finishes either at the end of the switching period (new ON interval) or when $x(t)$ reaches the extreme point $x = 1$, because the inductor current becomes positive. Apart from the trivial solution $y(t) = 0$, the dynamics in this interval is governed by the following 1D differential equation

$$\frac{dx}{dt} = -\frac{p}{x}, \tag{3}$$

whose solution is $x(t) = \sqrt{x^2(0) - 2pt}$.

2.1. *Implicit discrete-time model (stroboscopic 1D map)*

A natural way to study a system which uses a periodic excitation is by means of a discrete-time stroboscopic map relating the state variables at time instants $(n+1)T$ to those at time instants nT being $n \in \mathbb{N}$. Under DCM operation, let $(x_0, 0)$ be the system state when the cycle starts (ON topology) and because current at the end of the cycle is zero, let call by convenience $(x_3, 0)$ that state (just when ON starts again). Then, the stroboscopic map S is defined such that $x_3 = S(x_0)$. Note that in general, the state of the system can be (x_0, y_0) at the beginning of a switching cycle and (x_3, y_3) at its end, so due to DCM operation one has $y_3 = y_0 = 0$. A point x^* is said to be a fixed point of map S whenever it fulfills the equation $S(x^*) = x^*$.

In Fig. 2(b-c), an example of limit cycle in DCM, where $x_0 = x^*$ is a fixed point for the stroboscopic map S, is shown. In the panel (b) of this figure, the cycle is represented in the state plane. In the panel (c), the oscillogram covers just one period, starting at $(x_0, 0)$ and so finishing at the same state.

To analyze the dynamics driving to a limit cycle or periodic orbit, let us first consider the ON dynamics along time $t_1 = DT$. Integration of the state equations corresponding to the ON case, with initial conditions $(x(0), y(0))$ gives the explicit result (note that if $u = 1$, variables x and y can be integrated separately in (2))

$$x(t) = \sqrt{x^2(0) - 2pt}, \qquad y(t) = y(0) + t. \tag{4}$$

Then, if $(x(0), y(0)) = (x_0, 0)$, the state after the ON interval is as follows

$$(x_1, y_1) = \left(\sqrt{x_0^2 - 2pt_1}, t_1\right). \tag{5}$$

After that, the OFF dynamics ($u = 0$) takes place and numerical integration is needed in (2). The time instant t_2 (initial time $t = 0$ is reconfigured at the beginning of this new topology) is obtained by an event stop of the integration for $y(t) = 0$, thus giving time t_2 such that $y_2 = y(t_2) = 0$ with corresponding $x_2 = x(t_2)$.

Finally, the last interval, during which $y = 0$, lasts a time $t_3 = T - t_1 - t_2 > 0$, so the initial point $(x_0, 0)$ maps to $(x_3, 0)$, being $x_3 = S(x_0) = \sqrt{x_2^2 - 2pt_3}$, after period T. The limit cycle is obtained by applying the cyclic condition $x_3 = S(x_0) = x_0$.

Note that since explicit expressions for the orbit in the OFF topology are not available, we cannot have an exact expression for the stroboscopic map $S(x)$, and hence for its corresponding fixed points, i.e., states $(x^*, 0)$ mapping to $(S(x^*) = x^*, 0)$. Stable limit cycles can be determined by direct long time integration of the system differential equations but unstable limit cycles cannot be located in this way. To determine both stable and unstable limit cycles, ad hoc routines have been implemented using MAPLE software.

3. Limit cycles: Boundaries for existence and stability

Foundations for the existence or not of limit cycles in system (2)-(3) with power parameter p, and a periodic exciting signal for its control u, with parameters T, D as its period and duty ratio, is not a trivial subject

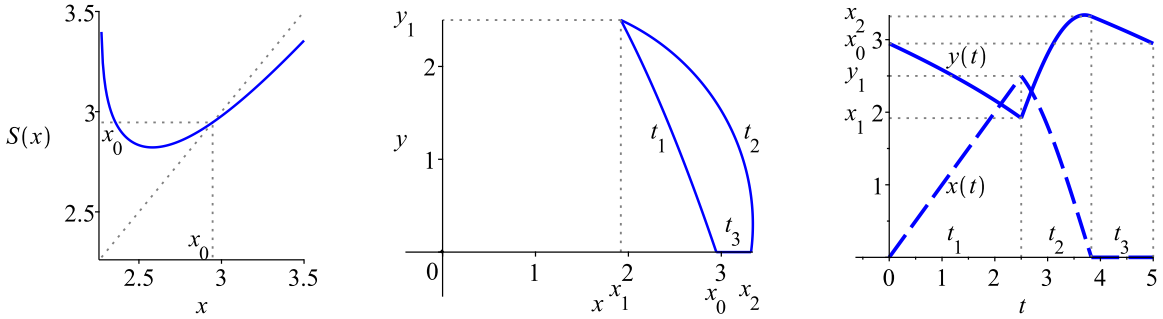

(a) (b) (c)

Fig. 2. DCM stroboscopic map S in (a) and limit cycle representations: (b) in the state space, (c) time-domain waveform. Parameters are $p = 1, t_1 = 2.5, T = t_1 + t_2 + t_3 = 5$, with resulting fixed point from $S(x^*) = x^*$: $x^* = 2.946322$.

as it will be shown in this paper. Only in one case an exact expression for a boundary of existence in the parameter space can be given, in other cases at most only approximated expressions can be obtained. Recall that p, T and t_1 are the system dimensionless parameters, such that $D = t_1/T$, and let also define a combined dimensionless parameter $K = 2p/T$.

3.1. *Existence condition $K > D^2$*

Let start by the only boundary that can be exactly determined from (2)-(3). Let $(x_0, 0)$ be the state at the beginning of a cycle, with $x_0 >> 1$ large enough in order to permit some approximations. After the ON topology along time $t_1 = DT$, from (4) the state is

$$x_1 = \sqrt{x_0^2 - 2pt_1} \approx x_0 - \frac{pt_1}{x_0}, \quad y_1 = t_1.$$

Along the OFF topology that is with $u = 0$, assuming constant $x = x_0$ in the term $-p/x$ as $x_0 >> 1$, the dynamics can be approximated by an ideal oscillation

$$x(t) \approx 1 + \sin(t)(t_1 - \frac{p}{x_0}) + \cos(t)(x_1 - 1), \tag{6}$$

$$y(t) \approx \frac{p}{x_0} + \cos(t)(t_1 - \frac{p}{x_0}) - \sin(t)(x_1 - 1), \tag{7}$$

valid during a short time interval $t \le t_2$, until event condition $y(t_2) = 0$. Then, by considering $\sin(t) \approx t$ and $\cos(t) \approx 1 - t^2/2$ in (6), it results

$$t_2 \approx \frac{t_1}{x_1 - 1}, \tag{8}$$

$$x_2 \approx x_1 + t_2\left(t_1 - \frac{p}{x_0}\right) - \frac{t_2^2(x_1 - 1)}{2} = x_0 - \frac{pt_1}{x_0} + \frac{t_1^2}{2(x_1 - 1)} - \frac{pt_1}{x_0(x_1 - 1)}. \tag{9}$$

Finally, in the third time interval, for which both the transistor and diode are open, along time $t_3 = T - t_1 - t_2$,

$$S(x_0) = x_3 = \sqrt{x_2^2 - 2pt_3} \approx x_2 - \frac{pt_3}{x_2}.$$

Taking into account that differences between the values (x_0, x_1, x_2), when x_0 is large enough, are very small (less than 1), the approximate stroboscopic map results

$$S(x) \approx x - \frac{pT}{x} + \frac{t_1^2}{2(x - 1)}. \tag{10}$$

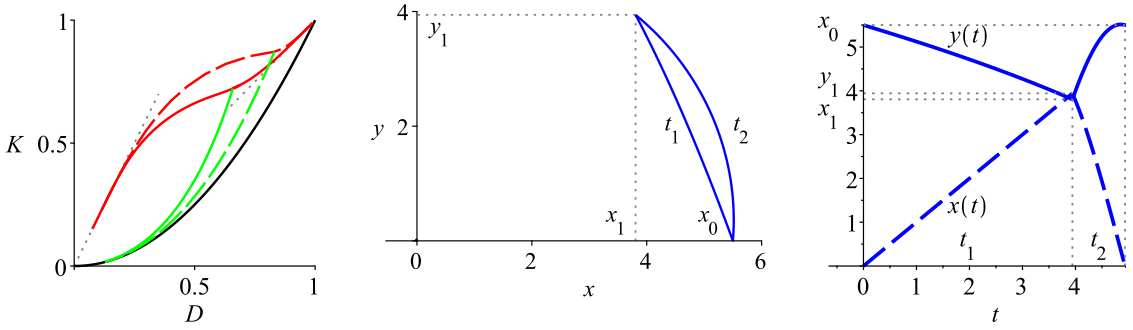

(a) (b) (c)

Fig. 3. (a) Boundary lines in the parameter plane (D, K) colored in black, red and lime, which account for $K = D^2$, CCM-DCM and period doubling bifurcations respectively; also, the continuous lines stand for $p = 2$, the dashed ones do for $p = 4.5$ and the dotted lines, $K = D$ and $K = 2D$ are asymptotes for the CCM-DCM limit. Illustrative critical CCM-DCM limit cycle with $p = 2, x^* = 5.5$, given with $T = 4.935067, t_1 = 3.942412$ ($D = 0.798857, K = 0.810526$), is depicted in the state plane (b) and time-domain waveform (c).

Then, from the limit cycle or fixed point condition $S(x) = x = x^*$, it is deduced that

$$x^* \approx \frac{2pT}{2pT - t_1^2} = \frac{K}{K - D^2}. \tag{11}$$

The above expression, which is valid only for K values higher than D^2 demonstrates that limit cycles cannot exist if $K < D^2$, being then $K = D^2$ a boundary in the parameter space. Black line in Fig. 3(a) corresponds to this boundary.

3.2. *Boundary with continuous conduction mode*

The other main boundary of existence for limit cycles is due to the extinction of the DCM. This frontier implies that $y(t) > 0$ for $0 < t < T$, and at the final instant the trajectory hits the abscissa, that is $y(T) = 0$. Actually, at the boundary CCM-DCM, a corner collision [di Bernardo et al., 2001] occurs: $y(t)$ becomes null at the end of the cycle just before starting again the ON topology, that is $t_3 = 0$ or equivalently $t_2 = T - t_1$, and so $x_2 = x_0$.

This boundary can be numerically computed for each selected parameter p and state $(x_0, 0)$, by reverse time integration of the differential equations corresponding to the OFF topology from $(x_0, 0)$ until the trajectory collides with the line $x = \sqrt{x_0^2 + 2py}$, associated to the ON dynamics, at the time instant $t = -t_2$. If (x_1, y_1) is this crossing point, then the parameters for the corner collision bifurcation at $(x_0, 0)$ with fixed p are $T = t_1 + t_2$ with $t_1 = y_1$. Lines in red color shown in Fig. 3(a) correspond to this boundary for two selected values $p = 2$ and $p = 4.5$. Also, an illustrative example of CCM-DCM boundary cycle, with parameters given in the caption, is in panel (b) of the same figure.

As can be appreciated in Fig. 3(a), the CCM-DCM boundary tends asymptotically to lines $K = 2D$ or $K = D$ if these parameters tend to 0 or 1 respectively for any value of parameter p.

The $K = 2D$ approximation is given for small values of K and D, that is to say for very large values of period T. This circumstance occurs when the trajectory corresponding to the OFF topology becomes close to the corresponding equilibrium point $(1, p)$. Actually, this happens for a fixed point x_0 near the critical value $x_c = \sqrt{1 + 2p^2}$ and parameter $t_1 \approx p$, because the ON trajectory ends around $(1, p)$. Taking into account the definitions of both parameters, the approximation $K/D \to 2$ is concluded.

The case $K = D$ is given when $x_0 >> 1$ is assumed, then from (8) and condition $t_3 = 0$, it is deduced that period T is hardly higher than t_1, that is the duty ratio D approaches 1. Besides, if the boundary and fixed point conditions are applied in (9), that is $x_2 = x_0$, after some approximations, the parameter

restriction $t_1 \approx 2p$, is deduced, and therefore, the asymptotic behavior $K = D$ is obtained. In Fig. 3(b-c), parameters for an illustrative example of critical limit cycles in the CCM-DCM boundary is given and also represented in the panels (b) and (c) using state space and time-domain waveforms respectively.

3.3. *Stability limit: smooth period doubling bifurcation*

A map qualitatively similar to the one depicted in Fig. 2(a) is found in a wide region of the parameter space, although more complex cases, mainly for low values of power p and high period T, are possible and will be examined later.

As is well known, the slope of S at x^*, also called characteristic multiplier m of the 1D map S

$$m = \left.\frac{dS}{dx}\right|_{x=x^*}, \tag{12}$$

determines the stability of the fixed point, such that it is asymptotically stable whenever $|m| < 1$. In the particular case that (12) is applied to the approximated expression $S(x)$ in (10) at the fixed point in (11), the approximate characteristic multiplier can be expressed as

$$m \approx 1 + \frac{pT}{x^{*2}} - \frac{t_1^2}{2(x^*-1)^2} \approx 1 - \frac{T^2(K-D^2)^3}{2KD^2},$$

then, close to the boundary $K = D^2$, $x^* \to \infty$ and $m \to 1$ (being $m < 1$).

If the parameters are varied moving away from that boundary, thus lowering the value of the fixed point x^*, two facts occur at the same time. On one hand, the characteristic multiplier goes progressively down from 1, and if the critical value $m = -1$ is overtaken, then the limit cycle becomes unstable via a smooth period doubling, also called flip, bifurcation. Besides this, the boundary CCM-DCM is approached and, if reached, the DCM limit cycle is extinguished. It depends on how parameters are varied, one or other boundary (DCM discontinuity or smooth period doubling bifurcation) is firstly attained.

In Fig. 3(a), the period doubling bifurcation boundary line is also plotted in lime color using the same parameters than for the CCM-DCM case. Note that in this (D, K) diagram, the stable period-1 orbit is bounded by the existence limits $K = D^2$ on the bottom and CCM on the top and by the stability period doubling bifurcation condition on the left. It can be also noticed that the stability region is progressively reduced as the parameter p increases.

As the smooth period-doubling bifurcation is of a codimension-1 type, in our three dimensional parameter space, two parameters (or mutual combinations) must be fixed and so the third parameter should be calculated in order to fit the critical condition $m = -1$. To do that, different parameters from the 3D parametric space can be used to obtain 1D boundary curves corresponding to the period doubling bifurcation boundary surface. In Fig. 3(a) some of these curves are shown. For each curve made with p fixed, t_1 is progressively varied, and for each pair (p, t_1), the corresponding critical period T has been obtained. To obtain this critical parameter, a numeric MAPLE routine, which input is the fixed state x^* and the output is the merit value $r = m + 1$, is progressively iterated, in such a way that x^* is recalculated to minimize r, thus approaching the period doubling bifurcation condition $m = -1$ as much as desired.

Let us pay attention to the intersection of nonsmooth CCM-DCM and smooth period doubling boundary surface in the 3D parameter space, which is a codimension-2 line. Two points of this line appear in Fig. 3(a), which are the crossing of corresponding lines for $p = 2$ and $p = 4.5$. To get any of these codimension-2 points, one parameter must be fixed and the other two parameters are calculated so as to simultaneously fulfill both CCM-DCM and smooth period-doubling conditions. Here, p has been fixed and the codimension-2 point is obtained by means of a numerical MAPLE routine similar to the one used for obtaining the point corresponding to the period doubling bifurcation. The difference here is that t_1 is not arbitrarily fixed, but it must fit the CCM boundary. The following results have been obtained: $T = 5.541362, t_1 = 3.649014, (D = 0.658505, K = 0.721844)$ with $x^* = 3.960434$ for $p = 2$, and $T = 10.323716, t_1 = 8.574694, (D = 0.830582, K = 0.871779)$ with $x^* = 8.844205$ for $p = 4.5$.

It is worth to note that after the smooth period doubling bifurcation takes place, an ulterior period-doubling cascade emerges, finally leading to chaotic behavior. This scenario, which is covered in [Benadero et al., 2020], is out of the scope of this work, devoted only to bifurcations of period-1 limit cycles.

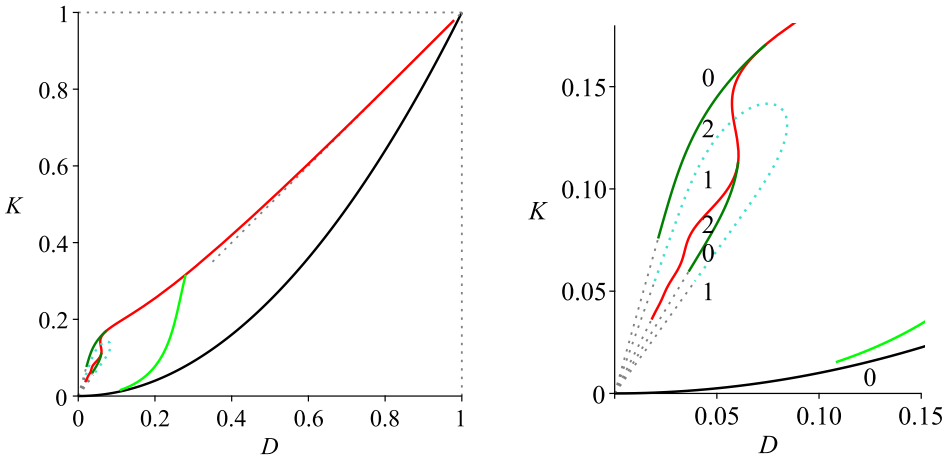

Fig. 4. (a) Boundary lines with fixed $p = 0.5$ in (D, K) plane, drawn in solid black, red, lime, green and dotted turquoise color, accounting for $K = D^2$, CCM-DCM, period doubling, fold and $x = 1$ bifurcation respectively. Zoom details are in (b).

It should be also mentioned that limit cycles associated to large periods, or expressed in other terms for low values of K, involve some degree of vicinity to OFF equilibrium $(1, p)$, and because it is unstable, the limit cycle eventually can approach $x = 0$ so much that system (2) cannot be solved. Due to this circumstance, part of the boundary lines are difficult to be obtained if K approaches 0 and if known, their asymptotic behavior is depicted instead.

3.4. *Bifurcation pattern and critical values of parameter p*

The pattern for existence and stability boundaries of the DCM period-1 limit cycle is fully described with power parameter p higher than the critical value $p_{c1} = 2$, as shown in Fig. 3(a). Note that if $p \geq p_{c1}$, the CCM-DCM boundary is encased between $K = D$ and $K = 2D$ asymptotes, and the limit cycle exists between that boundary and the boundary $K = D^2$, which does not depend on p. Concerning stability, the period doubling bifurcation boundary divides this region, the up-right one being stable. However, as it will be shown, if $p < p_{c1}$ new existence and stability boundaries emerge. Actually, the complexity of bifurcation pattern increases as p is further reduced below successive critical values of this parameter, some of which will be mentioned later. It is worth noting that the limit cycles involved in these new scenarios are likely not practical from the point of view of applications of switching converters, but are of interest considering the richness of dynamics involved.

The first critical power parameter value $p_{c1} = 2$, is related to the fact that the eigenvalues for the OFF-equilibrium point $(1, p)$ change from real to complex conjugate. These eigenvalues are $\lambda = \left(1 \pm j\sqrt{1 - 4p^2}\right)/(2p)$ with $j = \sqrt{-1}$. If $p < 2$, they become complex conjugate and so this equilibrium is an unstable focus. Qualitatively, the spiral behavior around the equilibrium can sustain an increasing number of turns around this focus as p is reduced below p_{c1}. It is not a surprising fact that in this case, the complexity of the bifurcation scenarios for period-1 limit cycle increases progressively when p is reduced. The first appearing bifurcation if $p < p_{c1}$ is a smooth fold, also called saddle-node, bifurcation that emerges from the CCM-DCM boundary as described below.

3.5. *Smooth fold bifurcation as an existence and stability limit for p < 2*

Unlike the monotone approach of the CCM-DCM boundary line to asymptote $K = 2D$ when $p > 2$, if $p < 2$, this line oscillates around the asymptote, with increasing amplitude as p is further reduced, due to the spiral character of the OFF-equilibrium. Actually both oscillations, the dynamics around the OFF equilibrium and the boundary line in the parameter space are closely related to each other. Furthermore,

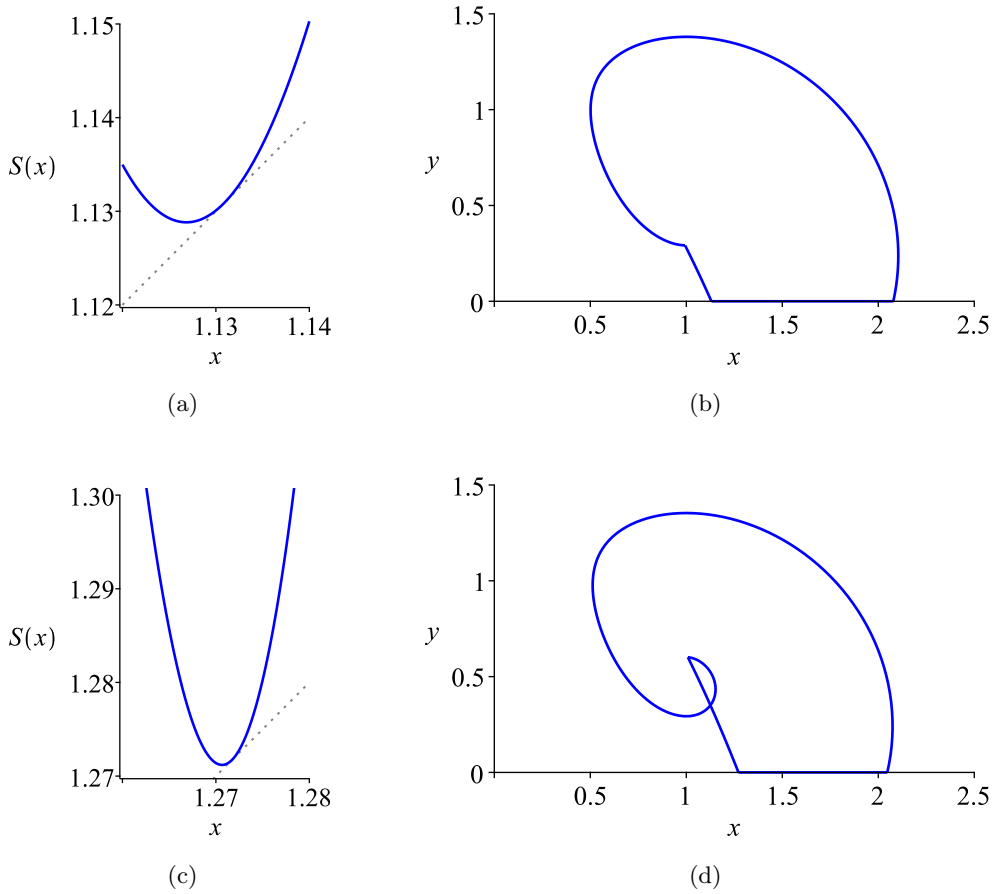

Fig. 5. Two examples of the stroboscopic map (a,c) and limit cycle (b,d) at the smooth fold bifurcation for $p = 0.5$: in (a-b) $T = 8.8$ with $t_1 = 0.291681$ ($D = 0.033146, K = 0.113636$), $x^* = 1.130821$; in (c-d) $T = 11.8$ with $t_1 = 0.600811$ ($D = 0.050916, K = 0.084746$), $x^* = 1.271724$.

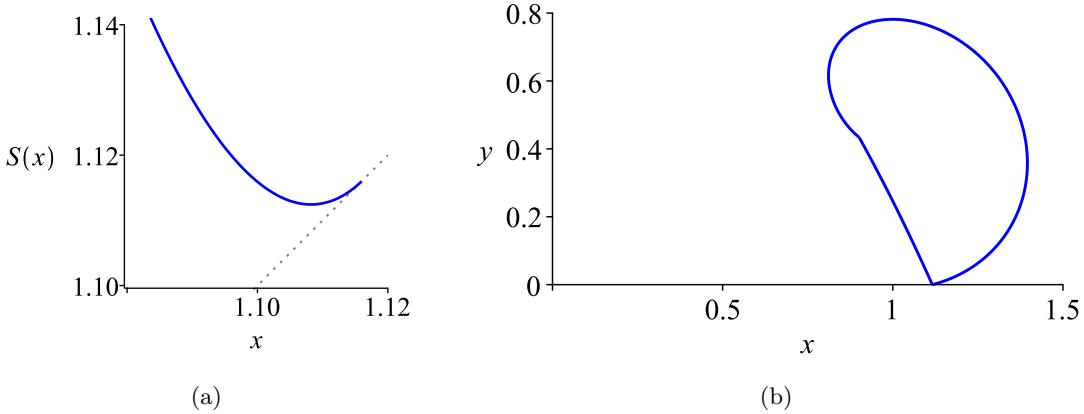

Fig. 6. (a) Stroboscopic map and (b) limit cycle at the smooth fold and nonsmooth CCM-DCM codimension-2 bifurcation for $p = 0.5$, thus being $D = 0.074057, K = 0.170683$ with $x^* = 1.116202$.

a smooth codimension-1 fold bifurcation line emerges from each oscillation of the CCM-DCM existence boundary. In Fig. 5, the set of boundaries for existence and stability of the period-1 limit cycle with $p = 0.5$

have been plotted. Note the waving of the CCM-DCM limit and the new fold lines. To avoid a cumbersome diagram, only two of these lines have been outlined, but theoretically these lines accumulate as approaching to the origin in (D, K) parameter plane.

To get points of the codimension-1 either smooth or nonsmooth fold bifurcation lines under fixed parameter p, we have opted for T as second fixed parameter to be varied progressively. For each pair p, T, two convenient values of the third parameter t_1 are previously chosen, say t_a, t_b, and for each one of them, maps S_a, S_b are estimated in a convenient x-domain. If properly chosen this domain, the functions $S_a(x) - x$ and $S_b(x) - x$ will have a minimum value inside it, say for values x_a and x_b respectively, that is $S'_a(x_a) = S'_b(x_b) = 1$, where $S' = dS(x)/dx$. Then the rated values $r_a = S_a(x_a) - x_a$ and $r_b = S_b(x_b) - x_b$ evaluate the vicinity to the fold bifurcation and from them, a new value $t_c = t_b - r_b(t_b - t_a)/(r_b - r_a)$ is considered. Following the same procedure, corresponding map S_c, variable x_c and rate r_c are deduced and after more repetitions, parameter t_1 with corresponding fixed point x^* will be determined with the desired precision, according to the selected threshold for rate r.

Analogous to the smooth period-doubling case, the smooth fold bifurcation manifold is born from the CCM-DCM one, although in this case, they converge tangentially in a codimension-2 bifurcation line. The point of this line when p is fixed can be computed similarly to the period doubling bifurcation case. Two convenient points x_a, x_b are selected as fixed points, then t_1, T are calculated for each of these points to meet CCM-DCM boundary, as described in the above section. After that, corresponding maps S_a, S_b are found and from them, rates $r_a = S'_a(x_a) - 1$ and $r_b = S'_b(x_b) - 1$ evaluates the neighborhood of x_a, x_b with corresponding t_a, T_a and t_b, T_b to the desired codimension-2 point. Repeating recursively the procedure, x_c, x_d... points are used, until getting the minimum desired rate r. For the value $p = 0.5$ used in Fig. 4, these critical points are $T = 5.858799, t_1 = 0.433887, (D = 0.074057, K = 0.170683)$ with $x^* = 1.116201$ and $T = 8.840806, t_1 = 0.534107, (D = 0.060414, K = 0.113112)$ with $x^* = 1.281624$ for the two branches depicted. The stroboscopic map and the limit cycle for the first of these two bifurcations are represented in Fig. 6. Note that DCM condition applies only on the left side of the fixed point, so only this part has been shown in the stroboscopic map.

Another interesting fact is that one of the two limit cycles generated at the smooth fold bifurcation is stable. However, this limit cycle can become unstable via a smooth period-doubling bifurcation by moving a small distance apart from the smooth fold bifurcation. With p fixed, the period doubling boundary has been computed and found so close to the fold one that it has not been included in the diagrams.

3.6. *Existence boundary at $x^* = 1$*

Concerning the existence of period-1 DCM limit cycles, if by varying parameters, a fixed point eventually reaches the critical state $(1, 0)$, that is $x^* = 1$, beyond that point the limit cycle is extinguished. Recall that under OFF dynamics, $dy/dt = 1 - x$, so that $dy/dt = 0$ for $x = 1$, which implies a visible tangency [Jefferies, 2009] at $(1, 0)$ state. Consequently, normal OFF topology is restored if $x(t)$ reaches the bound $x = 1$ before the end of the cycle, thus implying $y > 0$. In Fig. 7(a), three trajectories appear, the upper one is full OFF case, the bottom one enters the third time interval ($y = 0$) escaping just at the bound $(1, 0)$ and the middle one is the critical tangent trajectory. One example for this boundary is the limit cycle represented in Fig. 7(b).

The limit $x^* = 1$ can only be reached under certain conditions. Before determining these conditions, let see that the slope continuity at the ON to OFF transition state, that is dy/dx coincides for $u = 0$ and $u = 1$ at that state, requires the condition $y = t_1 = p$. By applying the equality of both slopes in (2), particularized at $u = 0$ and $u = 1$, the condition $y = p$ is obtained. Considering also that accordingly to (5) $y = t_1$, the slope continuity ON to OFF takes place under the condition $t_1 = p$. By a trial and error procedure, we have found the critical value $p_{c2} \approx 0.52135241$ such that if $p > p_{c2}$, even if $t_1 = p$, the OFF orbit reaches $x = 0$ natural limit an so it does not make sense. If $p < p_{c2}$, then x^* is reachable in a t_1-domain around p. The extreme values of this domain can be obtained by approaching $x = 0$ in the OFF dynamics as much as desired. For $p = 0.5$, one has $t_{lim1} < t_1 < t_{lim2}$ with $t_{lim1} \approx 0.356822$ and $t_{lim2} \approx 0.715570$. When approaching these limits, the period T increases progressively, then making D and K tending to zero while maintining practically constant the ratio K/D which converges to $2p/t_{lim}$, with

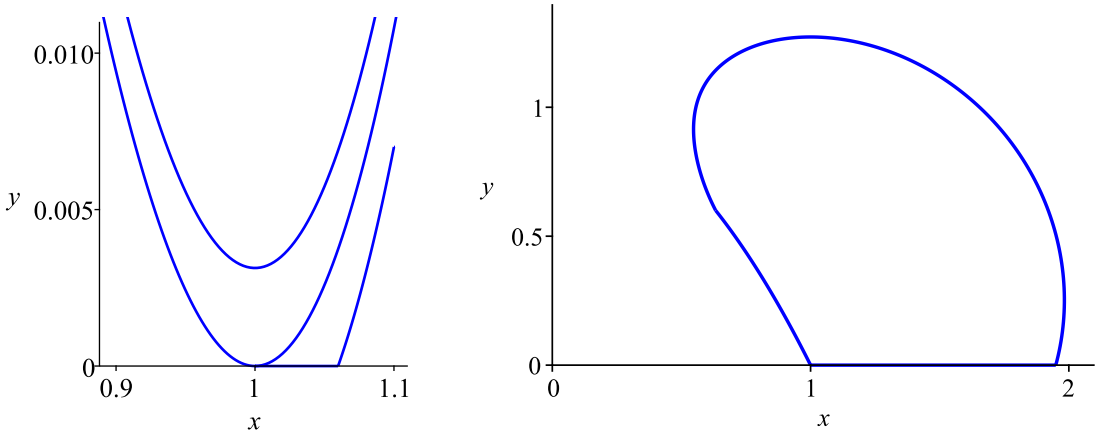

Fig. 7. Using $p = 0.5$, (a) set of trajectories near critical state (1,0) and (b) critical limit cycle for $x^* = 1$ with $t_1 = 0.6$, thus being $T = 7.249421$ ($D = 0.082765, K = 0.137942$).

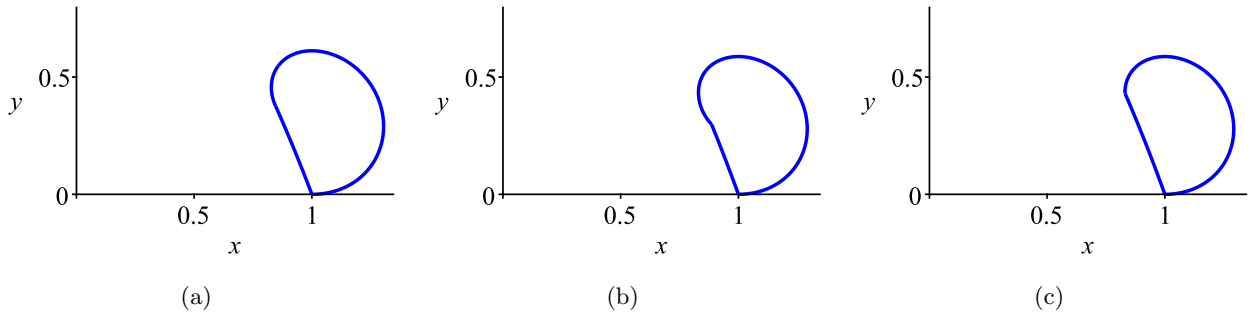

Fig. 8. Limit cycles at CCM-DCM and $x^* = 1$ boundaries: (a) critical case $t_1 = p = p_{c3} \approx 0.37785857$ with $T = 5.38779248$; $p = 0.36$ in (b-c) with $t_1 = 0.298926, T = 5.740569$ in (b) and $t_1 = 0.430882, T = 4.990133$ in (c).

t_{lim} equal to one of the two extremes of t_1-domain.

The dotted turquoise line in Fig. 4, which accounts for this bound under constant parameter $p = 0.5$, has been obtained by varying progressively t_1 in its valid domain, and for each pair (p, t_1), the critical limit cycle and its period are determined in the standard form, by selecting $x^* = 1$ as the fixed point.

The number of fixed points (either stable or unstable) appears indicated in Fig. 4(b) for regions defined by boundaries exposed so far. Note that two limit cycles emerge from the fold line and one limit cycle extinguishes at the two boundaries CCM-DCM and $x^* = 1$. Also, regarding the CCM-DCM case, the direction for which the fixed point appears is inverted at its codimension-2 bifurcation with the smooth fold one.

Up to this point, two qualitative changes in the possible set of bifurcations have been exposed when decreasing p. The first and most relevant case occurs at $p = p_{c1}$, with $p_{c1} = 2$, such that when $p < p_{c1}$, the codimension-1 smooth fold bifurcations linked to the nonsmooth CCM-DCM bifurcation, emerge. The second case at $p = p_{c2}$, with $p_{c2} \approx 0.52135241$, implies the emergence of codimension-1 nonsmooth boundary due to overpassing the DCM limit ($x^* = 1$).

A third critical value $p_{c3} \approx 0.37785857$ occurs when $x^* = 1$ at CCM-DCM boundary, being also $T \approx 5.38779248$ and $t_1 = p_{c3}$ ($K \approx 0.14026471, D = K/2$). This critical limit cycle, which is shown in Fig. 8(a), features simultaneously: CCM-DCM boundary, which is also placed at $x^* = 1$ and slope continuity at ON to OFF transition (that is with $t_1 = p$).

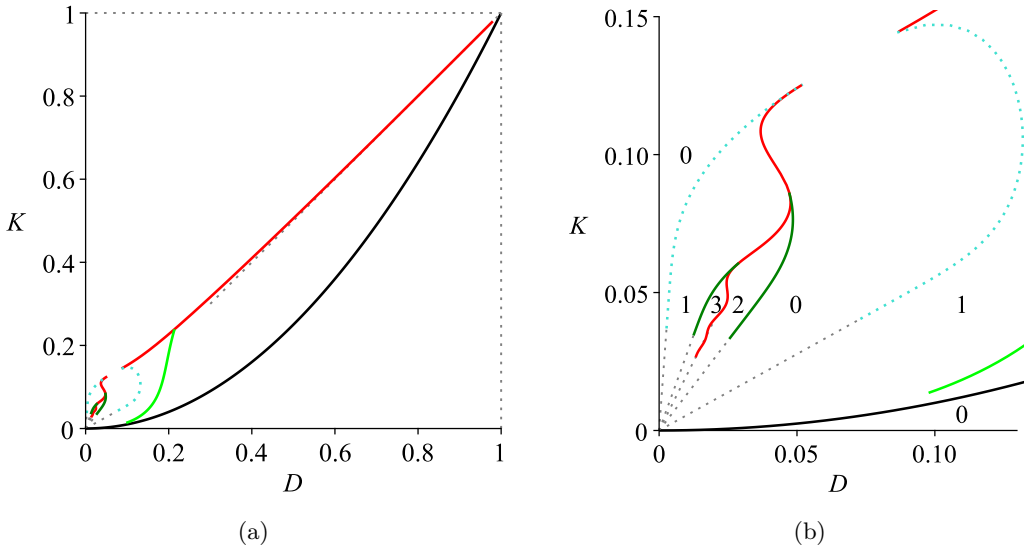

Fig. 9. (a) Boundary lines with fixed $p = 0.36$ in (D, K) plane in solid black, red, lime, green and dotted turquoise accounting for $K = D^2$, CCM-DCM, period doubling, fold and $x^* = 1$ bifurcation respectively. Zoom details are in (b), also including the number of limit cycles in some parameter regions.

If $p < p_{c3}$, the CCM-DCM boundary line splits due to the interaction with $x^* = 1$ bound, as it can be appreciated in Fig. 9 by using $p = 0.36 < p_{c3}$. Limit cycles at the extremes of the two trams in which the CCM-DCM boundary is split are given in Fig. 8(b-c).

Due to the enhancement of the spiral behavior as decreasing p, the DCM-CCM boundary line is further splitting for lower values of p, for instance one extra section appears if $p \lesssim 0.24718118$.

Let us go back to the t_1-domain defining the $x^* = 1$ boundary line limit, as it can be seen in Fig. 4. In this example, by using $p = 0.5$, $t_1 \approx 0.356822$ is the lower limit of the domain. Recall that $p_{c2} \approx 0.52135241$ is a critical value, such that if $p < p_{c2}$, a t_1-domain for this boundary is defined. This domain gets larger when p decreases. Actually, for a new critical value of the parameter, say $p_{c4} \approx 0.33095806$, it is found that there is not a lower limit for the t_1-domain. This critical value is associated to the fact that if $p < p_{c4}$, then the OFF trajectory starting at the bound state $(1, 0)$ evolves around the corresponding equilibrium without divergence as decreasing x, thus being a valid trajectory. Conversely, if $p_{c4} < p < p_{c3}$, a minimum value for t_1 is necessary to prevent approaching $x = 0$.

Figure 10, using $p = 0.32 < p_{c4}$, shows two new kind of existence boundaries in the parameter space that emerge when $p < p_{c4}$ and will be detailed below. These extra nonsmooth boundaries appear only if the OFF trajectory starting at the bound state $(1, 0)$ is defined, and this is only possible if $p < p_{c4}$ and somehow long driving signal periods.

3.7. *Boundary with* off *trajectory tangent at* $(1, 0)$

One of these new boundaries, which is depicted in Fig. 10 with solid dark blue line, is associated to critical limit cycles obtained as follows. The OFF trajectory is computed starting from the critical point $(1, 0)$ both in forward and reverse time directions. Let $t_P(p)$ be the positive time at which the trajectory hits abscissa at $(x_P(p), 0)$ state and (x_1, y_1) be the state obtained by the reverse computation using an arbitrary time $-t'$. From (x_1, y_1) determination, the ON time and the fixed point are straightforward: $t_1 = y_1$ and $x^* = \sqrt{x_1^2 + 2pt_1}$. Finally, the cycle is completed in DCM from $x_P(p)$ to x^*, thus with a period $T = t_1 + t' + t_P(p) + \left(x_P(p)^2 - x^{*2}\right)/(2p)$.

In Fig. 11(a), the stroboscopic map with parameters in the caption shows clearly a nonsmooth bifurcation, with corresponding critical limit cycle in panel (b). On one side of the bifurcation (see the solid blue line in Fig. 10), the discontinuity of the map moves below bisector line (x), so that they will not define a fixed point. Conversely, on the other side, the two lines defining the discontinuity intersects with the

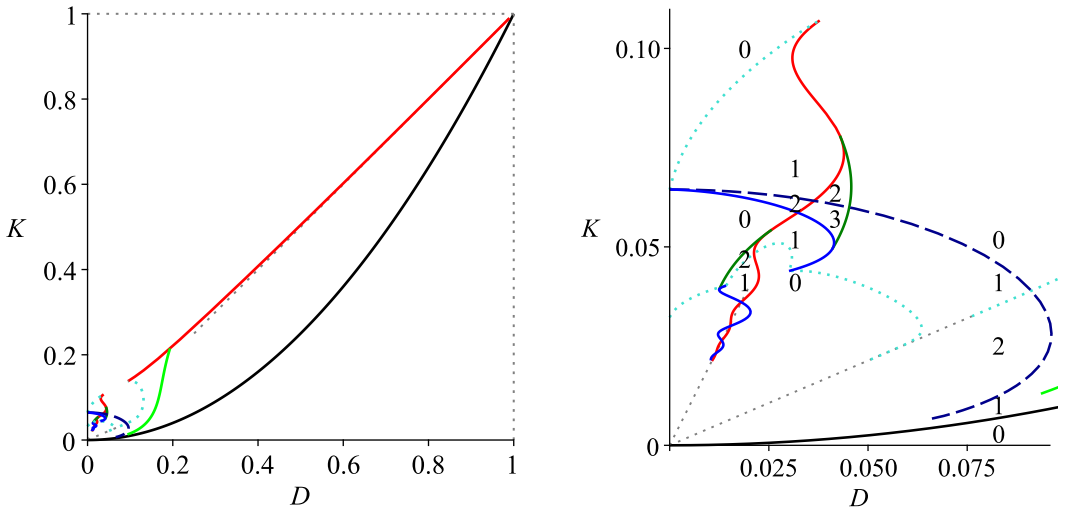

Fig. 10. (a) Boundary lines with fixed $p = 0.32$ in (D, K) plane. Solid black, red, lime, green and dark blue lines account for $K = D^2$, CCM-DCM, period doubling, smooth fold and nonsmooth cases, dotted turquoise and dashed blue do for $x^* = 1$ and $x^* = x_P(p)$ ones, respectively. Zoom in (b) includes the number of limit cycles in some parameter regions.

bisector x in two (fixed) points, with stability character depending on the slope $S'(x^*)$. However, following the same boundary, we can see in Fig. 11(c), the stroboscopic map shows also a discontinuity, but with only one fixed point at its two sides. The feature now is the different slope of $S(x)$, thus permitting a possible change of stability. The corresponding critical limit cycle is in panel (d).

Consequently, an interesting fact concerning this boundary line is the existence of a critical point belonging to it, which is responsible of its partition in two sections, each one with a map behavior as in panel (a) or in panel (c) of Fig. 11. Actually, this splitting point is codimension-2 bifurcation type, in which the smooth fold described earlier and nonsmoothness of this new boundary are born simultaneously. Parameter values of this critical point and its stroboscopic map with the discontinuity at the tangent point clearly visible is in Fig. 11(e), with corresponding limit cycle given in panel (f) of the same figure.

Another property of this boundary line is the fact that, due to the spiral behavior of the OFF trajectory, this line can be divided in segments. Note in Fig. 10, the solid blue line representing this case for $p = 0.32$ is divided in two disconnected parts by the $x^* = 1$ boundary. The limit cycles for the two extreme points are represented in Fig. 12.

Most of the limit cycles existing with low D and K parameter values when $p < p_{c1} = 2$, far from the the main smooth period-doubling boundary are unstable. For instance, those appointed in the panel (b) of Figs. 4,9,10. Nevertheless, after the smooth fold bifurcation occurs, one of the two emerging limit cycles is stable, although it maintains stability in a reduced range of the parameter space. Besides, after the boundary associated to the orbit tangency at $(1, 0)$ is crossed, another stable limit cycle can be born and even maintain stability in a larger parameter values region. In Fig. 13, the stroboscopic map, with parameter $p = 0.32$ and others in the caption, is shown. It can be clearly appreciated the existence of three fixed points, the central one with $x^* \approx 1.208639$ is unstable ($m \approx 2.8181 > 1$), but the other two ones are stable. These last are shown in panels (b-c) of the same figure including the values of x^* and m.

3.8. *Boundary with x_P as fixed point*

The second extra nonsmooth boundary, see the dashed light blue line in Fig. 10, is also linked to tangency at $(1, 0)$, but specifically with the fixed point $x^* = x_P(p)$ thus being another existence boundary of limit cycle. Note in Fig. 10(b) that this boundary line is born at the same point in the parameter space than the line with OFF trajectory tangent at $(1, 0)$ and the line for $x^* = 1$. This point where the three lines meet is defined with $D = 0$, thus meaning in practice the absence of exciting signal ($t_1 = 0$) and consequently the

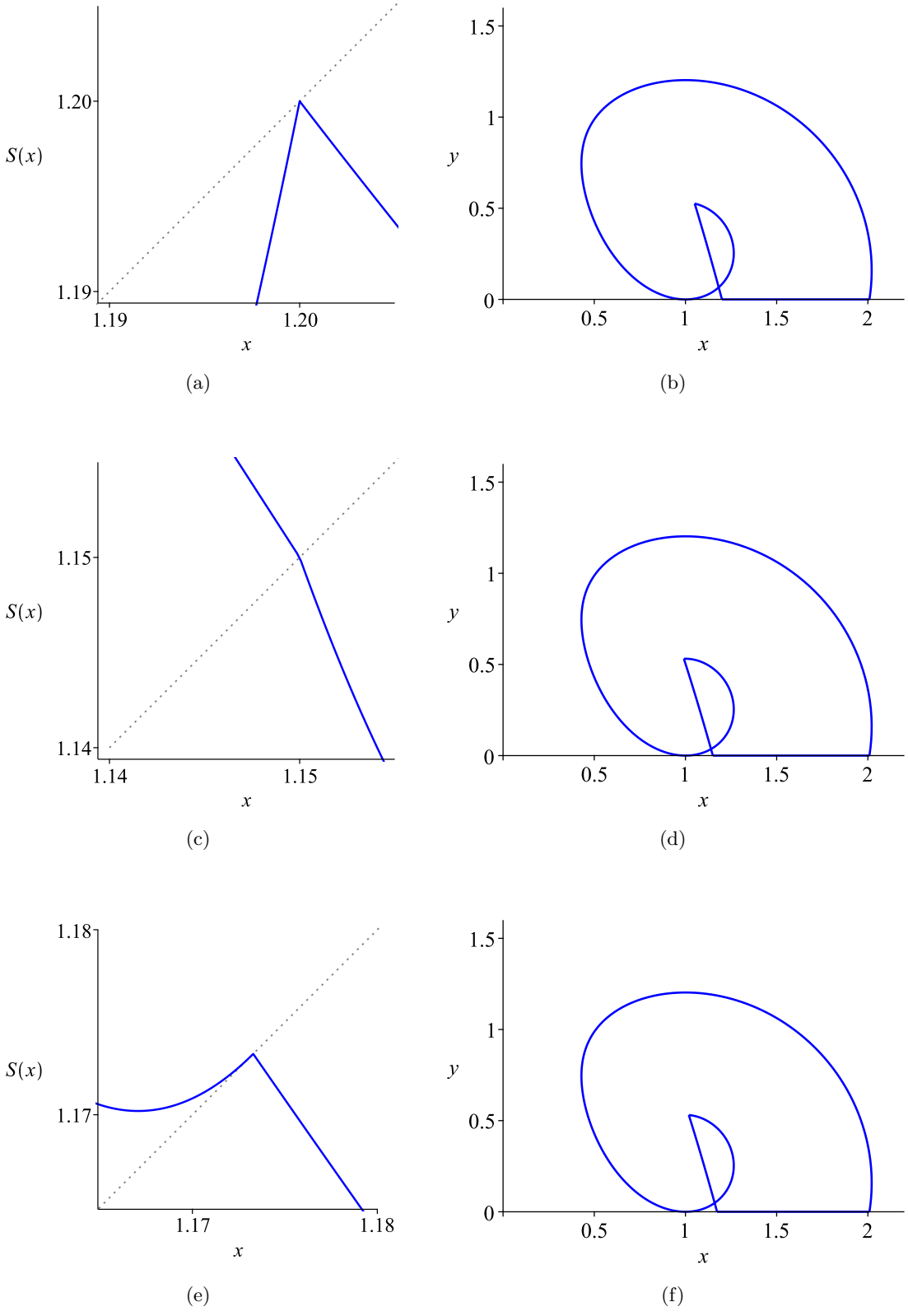

Fig. 11. Examples of the stroboscopic map (a,c,e) and limit cycle (b,d,f) with $p = 0.32$ at some bifurcating cases. Nonsmooth fold in (a-b) for $x^* = 1.2$, then $T = 12.700430, t_1 = 0.525447$ ($D = 0.041372, K = 0.050392$). Discontinuity in (c-d) for $x^* = 1.15$, then $T = 13.164305, t_1 = 0.531112$ ($D = 0.040345, K = 0.0486163$). Codimension-2 smooth and nonsmooth fold in (e-f) with $T = 12.951603, t_1 = 0.530508$ ($D = 0.040961, K = 0.049415$), being $x^* = 1.173290$.

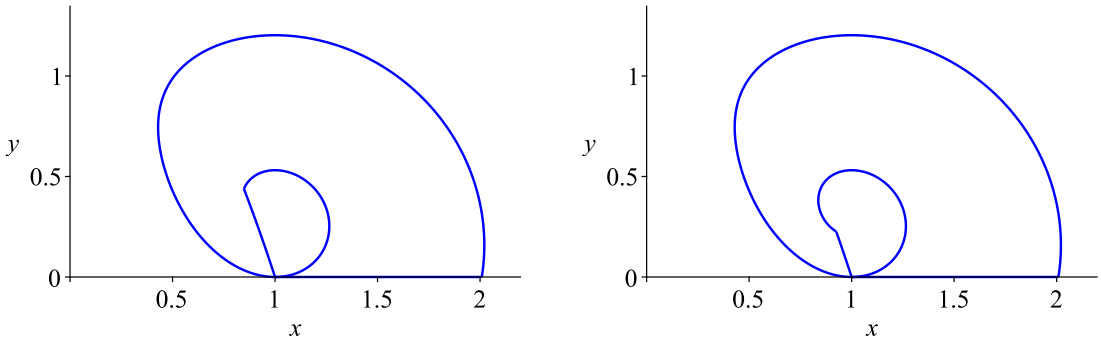

(a) (b)

Fig. 12. Critical limit cycles for $p = 0.32$ and double condition $x^* = 1$ and OFF trajectory tangent at the same point. Parameters are $D = 0.030081, K = 0.043914$ in (a) and $D = 0.014230, K = 0.040235$ in (b).

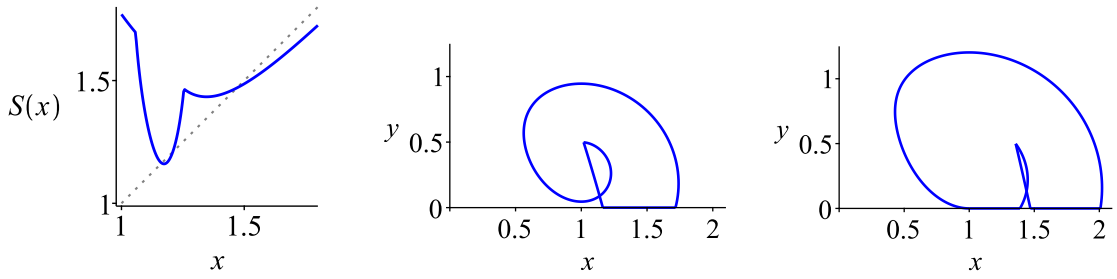

(a) (b) (c)

Fig. 13. Stroboscopic map in (a) under parameters $p = 0.32, D = 0.0443, K = 0.0569$. Corresponding stable limit cycles with $x^* = 1.163739, m = -0.6801$ in (b) and $x^* = 1.470005, m = 0.5157$ in (c).

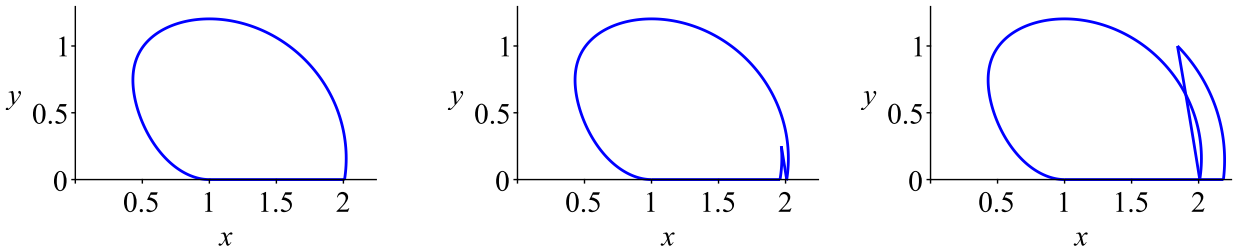

(a) (b) (c)

Fig. 14. Some critical cycles using $p = 0.32$. (a) the particular cycle $\mathcal{C}_P$ with $T = 9.930006, x_P = 2.008513$. Examples of boundary limit cycles $x^* = x_P$: $t_1 = 0.25, T = 10.128294$ in (b) and $t_1 = 1.0, T = 13.003655$ in (c).

system is autonomous under these conditions.

Definition 1. For a parameter $p < p_{c4}$ in absence of the driven signal $u(t)$, a particular limit cycle, called here $\mathcal{C}_p$, exists. This is the orbit defined by an OFF trajectory, see (2) with $u = 0$, running from bound state $(1, 0)$ until hitting the x-axis at the state $(x_P(p), 0)$ in time $t_P(p)$, and finally flowing with $y = 0$, see (3), to return at the initial state. The period of this cycle is $T_P(p) = t_P(p) + (x_P(p) - 1)^2/(2p)$.

The limit cycle $\mathcal{C}_p$, with parameter $p = 0.32$ is plotted in 14(a) with corresponding data in the caption. Two other limit cycles belonging to the boundary with x_P as fixed point are in panels (b,c) of the same figure.

It should also be noticed that each nonsmooth boundary whose critical limit cycles includes the bound state $(1, 0)$ theoretically replicates in many boundaries with the same properties. Actually, this property is a particular case of a more general result, as summarized in the following proposition.

Proposition 1. *For the system* (2)-(3) *with power parameter* $p < p_{c4}$ *and exciting signal with dimensionless switching period* T *and dimensionless* ON *time* t_1*, if an arbitrary state* (x_a, y_a) *maps to a state* (x_b, y_b) *that belongs to the particular limit cycle* $\mathcal{C}_P$*, any other driving signal with parameters* $T + nT_P$ *and* t_1*, where* T_P *is the period of* $\mathcal{C}_P$ *and* $n \in \mathbb{N}$*, will also map* (x_a, y_a) *to* (x_b, y_b)*.*

The proof is direct by considering that the state (x_b, y_b) after time T will be reproduced at the end of the driving signal, that is if (x_b, y_b) belongs to $\mathcal{C}_P$, after completing the period in the additional time nT_P, the orbit comes back to this same point. Note that for the fixed point of a limit cycle, we have the restriction $x_a = x_b = x^*, y_a = y_b = 0$, then if $1 \leq x^* \leq x_P(p)$, systems with the same parameters $p < p_{c4}$ and t_1, differing their periods on nT_P with n integer, will have the same fixed points and with the same stability character, whenever $x^* \in [1, x_P(p)]$.

Consequently, this property applies to nonsmooth boundaries related to tangency at $(1, 0)$ and also for $x^* = 1$ or $x^* = x_P$. However, to avoid cumbersome diagrams, these replicative boundaries have not been included in Fig. 10 except for two segments of the $x^* = 1$ boundary case (dotted turquoise line).

We see that decreasing p on one hand increases the area in the parameter plane (D, K) with a stable fundamental limit cycle, while on the other hand the boundaries for existence of period-1 limit cycles becomes more complex. We will only add here another occurrence in the bifurcation pattern. For the critical value $p_{c5} \approx 0.19518223$, being also $T \approx 7.95836864, t_1 \approx 0.83476363$, the nonsmooth boundary $x^* = 1$ becomes tangent to the smooth period doubling boundary so that if $p < p_{c5}$ this last bound is split by the $x^* = 1$ line.

3.9. *Effect of a parasitic series resistance and other non ideal features*

The analysis carried out up to now has been made out under ideal conditions that allow us a relatively simplified development. A possible deviation in a real implementation is the presence of a parasitic resistance, mainly in series with the inductor. Let R_S be its value, thus normalized as $r_S = R_S/Z_0$, so that the second differential expression in (2), takes the following modified form

$$\frac{dy}{dt} = -r_S y + (u - 1)x + 1.$$

The results in Fig. 15, with dimensionless parameter palue $p = 0.36$ and $r_S = 0.1$, show a qualitatively similar pattern than the ideal case with $r_S = 0$, see Fig. 9. Only small deviations in the critical lines can be appreciated.

Another case of interest is the ideal CPL behavior restricted to some regions of state variables, see for instance [Henao et al., 2022; Benadero et al., 2015] to get further details. As it was mentioned above, part of our analysis deals with interesting bifurcation patterns. The inclusion of a piecewise behavior of the load converter can be addressed in a future work, then revising the parameter regions in which the exposed bifurcations still persist and likely finding out new emerging bifurcation cases.

4. Conclusions

Existence and stability of fundamental limit cycles of an open loop DC-DC boost converter, with constant power load and operating in discontinuous conduction mode, has been analyzed via a 1D model with only three dimensionless parameters. Apart from the smooth period doubling bifurcation concerning the stability of the main limit cycle, different kind of boundaries for limit cycle existence, most of them nonsmooth, have been obtained. Several diagrams have been added to illustrate them and the result is a progressively more complex bifurcation pattern as the power parameter p decreases. Emphasis has been made in the intersection of the different boundaries, actually codimension-2 bifurcations, which are of great relevance in the diagrams. Also numerical data for the critical values of p at which new boundaries emerge and so the bifurcation pattern is qualitatively modified have been given.

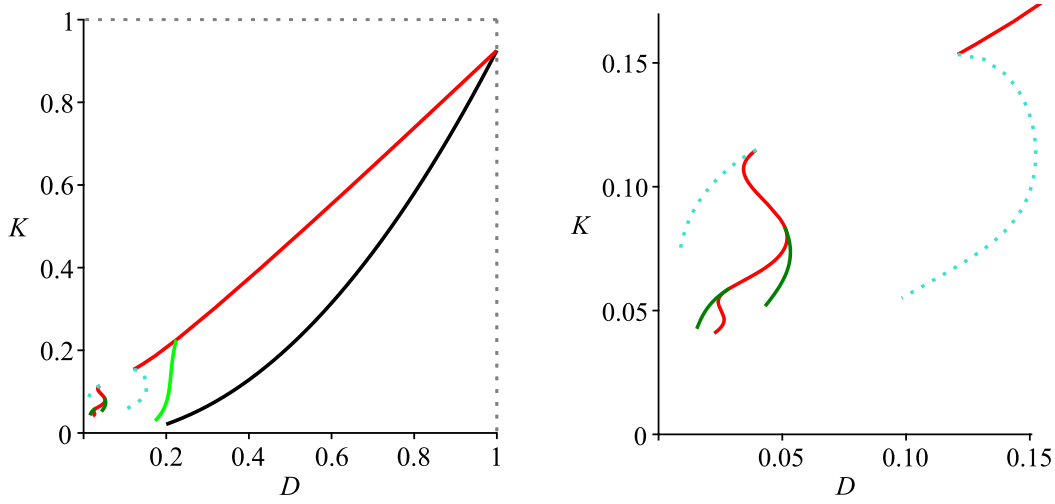

(a) (b)

Fig. 15. Critical lines, using the same color and style, with the same parameter value $p = 0.36$ than in Fig. 9 but taking into a normalized series resistance $r_S = 0.1$. Note that except from negligible deviations from the ideal case (Fig. 9), a very similar pattern can be observed.

Acknowledgements

This work has been partially sponsored by the Spanish *Ministerio de Ciencia e Innovación* under grants PID2020-120151RB-I00 and PID2019-111443RB-100. C. K. Tse acknowledges the support of Honk-Kong Research Grant Council under grant GRF 11207121.

References

Al-Nussairi, M. K., Bayindir, R., Padmanaban, S., Popa, L. M. & Siano, P. [2017] "Constant power loads (CPL) with microgrids: problem definition, stability analysis and compensation techniques," *Energies*, **10**, **1656**, 1–20.

Avrutin, V. & Zhusubaliyev, Z. T. [2020] "Piecewise-linear map for studying border collision phenomena in DC/AC converters, " *International Journal of Bifurcation and Chaos,* **30**, **7**, 2030015.

Banerjee, S. Ranjan P. & Grebogi, C. [2000] "Bifurcations in two-dimensional piecewise smooth maps-theory and applications in switching circuits," *IEEE Transactions on Circuits and Systems I: Fundamental Theory and Applications,* **47**, **5**, 633–643.

Banerjee S. & Verghese, G. C. [2001] *Nonlinear phenomena in power electronics — Attractors, Bifurcations, Chaos, and Nonlinear Control,* New York, IEEE Press.

Belkhayat, M., Cooley, R. & Witulski, A. [1995] "Large signal stability criteria for distributed systems with constant power loads," Proc. PESC'95, *Power Electronics Specialist Conference,* **2**, 1333–1338.

Benadero, L., Cristiano, R. Pagano, D. J. & Ponce, E. [2015] "Nonlinear analysis of interconnected power converters: A case study," *IEEE Journal of Emerging and Selected Topics in Circuits and Systems,* **5**, **3**, 326–335.

Benadero, L., El Aroudi, A., Martinez-Salamero L. & Tse, C. K. [2020] "Period doubling route to chaos in open loop boost converters under constant power Loading and discontinuous conduction mode conditions," *IEEE International Symposium on Circuits and Systems (ISCAS),* 1–5.

Bharadwaj, P. & John, V. [2014] "Direct duty ratio controlled MPPT algorithm for boost converter in continuous and discontinuous modes of operation," in *2014 IEEE 6th India International Conference on Power Electronics (IICPE),* 1–6.

Chakrabarty, K., Poddar, G. & Banerjee, S. [1996] "Bifurcation behavior of the buck converter," *IEEE Transactions on Power Electronics,* **11**, **3**, 439–447.

Chen, Y., Tse, C. K., Qiu, S. S., Lindenmuller L. & Schwarz, W. [2008] "Coexisting fast-scale and slow-scale instability in current-mode controlled DC/DC converters: Analysis, simulation and experimental results," *IEEE Transactions on Circuits and Systems I: Regular Papers,* **55**, **10**, 3335–3348.

Cheng, L. Ki, W. H., Yang, F., Mok, P. K. T. & Jing, X. [2017] "Predicting subharmonic oscillation of voltage-mode switching converters using a circuit-oriented geometrical approach," *IEEE Transactions on Circuits and Systems I: Regular Papers,* **64**, **3**, 717–730.

Chu, G., Tse, C. K. & Wong, S. C. [2009] "Line-frequency instability of PFC power supplies," *IEEE Transactions on Power Electronics,* **24**, **2**, 469–482.

Cristiano, R., Pagano, D. J., Benadero, L. & Ponce, E. [2016] "Bifurcation analysis of a DC–DC bidirectional power converter operating with constant power loads," *International Journal of Bifurcation and Chaos,* **26**, **4**, 1–18.

Cortes, J., Svikovic, V., Alou, P., Oliver, J. A., Cobos, J. A. & Wisniewski, R. [2015] "Accurate analysis of subharmonic oscillations of V^2 and $V^2 I_c$ controls applied to buck converter," *IEEE Transactions on Power Electronics,* **30**, **2**, 1005–1018.

Deane, J. H. B. & Hamill, D. C. [1990] "Instability, subharmonics, and chaos in power electronic systems," *IEEE Transactions on Power Electronics*, **5, 2**, 260–268.

di Bernardo, M. Budd, C. J. & Champneys, A. R. [2001] "Corner collision implies border-collision bifurcation," *Physica D,* **154**, **3-4**, 171–194.

El Aroudi, A. Debbat, M., Giral, R., Olivar, G., Benadero, L. & Toribio, E. [2005] "Bifurcations in DC-DC switching converters: Review of methods and applications," *International Journal of Bifurcation and Chaos,* **15**, **05**, 1549–1578.

El Aroudi, A., Haroun, R., Al-Numay, M. S., Calvente J. & Giral, R. [2021] "Fast-scale stability analysis of a DC–DC boost converter with a constant power load," *IEEE Journal of Emerging and Selected Topics in Power Electronics,* **9**, **1**, 549–558.

El Aroudi, A.; Debbat, M.; Giral, R.; Martinez-Salamero, L.[2001] "Quasiperiodic route to chaos in DC–DC switching regulators," in In Proceedings of the ISIE 2001. 2001 IEEE International Symposium on Industrial Electronics Proceedings, (Cat. No.01TH8570), Pusan, Republic of Korea, 12–16 June 2001; Volume 3, pp. 2130–2135.

El Aroudi, A., Mandal, K., Giaouris, D., Banerjee, S., Abusorrah, A., Al Hindawi, M. & Al-Turki, Y. [2016] "Fast-scale stability limits of a two-stage boost power converter," *International Journal of Circuit Theory and Applications,* **44**, 1127–1141.

Emadi, A., Khaligh, A., Rivetta, C. H. & Williamson, G. A. [2006] "Constant power loads and negative impedance instability in automotive sy, stems: Definition, modeling, stability, and control of power electronic converters and motor drives," *IEEE Transactions Vehicular Technology,* **55**, **4**, 1112–1125.

Fossas, E. & Olivar, F. [1996] "Study of chaos in the buck converter," *IEEE Transactions on Circuits and Systems I: Fundamental Theory and Applications,* **43**, **1**, 13–25.

Gain, G. & Banerjee, S. [2003] "Border-collision bifurcations in one-dimensional discontinuous maps," *International Journal of Bifurcation and Chaos,* **13**, **11**, 3341–3351.

Gavagsaz-Ghoachani, R., Martin, J. P, Pierfederici, S., Nahid-Mobarakeh, B. & Davat, B. [2013] "DC power networks with very lowvcapacitances for transportaion systems: Dynamic behavior analysis," *IEEE Transactions on Power Electronics,* **28**, **12**, 5865–5877.

Gavagsaz-Ghoachani, R., Saublet, L. M., Martin, J. P., Nahid-Mobarakeh, B. & Pierederici, S. [2017] "Stability analysis and active stabilization of DC power systems for electrified transportation systems taking into account the load dynamics," *IEEE Transactions on Transportation Electrification,* **3**, **1**, 3–12.

Giaouris, D., Banerjee, S. Zahawi, B. & Pickert, V. [2008] "Stability analysis of the continuous conduction mode buck converter via Filippov's method," *IEEE Transactions on Circuits Systems I,* **55**, **4**, 1084–1096.

Giaouris, D. Maity, S., Banerjee, S. Pickert, V. & Zahawi, B. [2009] "Application of Filippov method for the analysis of subharmonic instability in DC-DC converters," *International Journal of Circuit Theory and Applications,* **37**, **8**, 899–919.

Griffo, A. & Wang, J. [2012] "Large signal stability analysis of 'more electric' aircraft power systems with

constant power loads," *IEEE Transactions on Aerospace and Electronic Systems,* **48**, **1**, 477–489.

Hamill, D. C. [1995] "Power electronics: A field rich in nonlinear dynamics," in *Proceedings of the Workshop on Nonlinear Dynamics of Electronic Systems,* Dublin, Ireland, 28–29 July 1995, 164–179.

Henao, M., Cristiano, R. & Pagano, D. J. [2022] "Bifurcation analysis of 3D-PWS systems with two transversal switching boundaries: A case study in power electronics," *Physica D: Nonlinear Phenomena*, **442**, 133505.

Jeffrey, M. R. [2009] "Two-folds in nonsmooth dynamical systems," *IFAC Proceedings Volumes,* **42**, **7**, 81–86.

Kabe, T., Parui, S., Torikai, H., Banerjee, S. & Saito, T. [2007] "Analysis of piecewise constant models of current mode controlled DC-DC converters," *IEICE Transactions on Fundamentals of Electronics, Communication and Computer Siences,* **E90-A(2)**, 448–456.

Kwasinski, A. & Onwuchekwa, C. N. [2011] "Dynamic behavior and stabilization of DC microgrids with instantaneous constant-power loads," *IEEE Transactions on Power Electronics,* **26**, **3**, 822–834.

Leng, M. , Zhou, G. , Zhou, S. , Zhang, K. & Xu, S. [2018] "Stability analysis for peak current-mode controlled buck LED driver Based on discrete-time modeling," *IEEE Journal of Emerging and Selected Topics in Power Electronics,* **6**, **3**, 1567–1580.

Mandal, K. & Banerjee, S. [2015] "Synchronization phenomena in microgrids with capacitive coupling," *IEEE Journal on Emerging and Selected Topics in Circuits and Systems,* **5**, **3**, 364–371.

Middlebrook, R. D. [1976] "Input filter consideration in design and application of switching regulators," *Industry Applications Society annual Meeting*, 366–382.

Onwuchekwa, C. N. & Kwasinski, A. [2010] "Analysis of boundary control for buck converters with instantaneous constant-power loads," *IEEE Transactions on Power Electronics,* **25**, **8**, 2018–2032.

Papafotiou G. A. & Margaris, N. I. [2004] "Calculation and stability investigation of periodic steady states of the voltage controlled buck DC-DC converter," *IEEE Transactions on Power Electronics,* **19**, **4**, 959–970.

Rahimi, A. M. & Emadi, A. [2009] "An analytical investigation of DC/DC power electronic converters with constant power loads in vehicular power systems," *IEEE Transactions on Vehicular Technology,* **58**, **6**, 2689–270.

Rahimi, A. & Emadi, A. [2010] "Discontinuous-conduction mode DC/DC converters feeding constant-power loads," *IEEE Trans. on Industrial Electron.*, **57**, **4**, 1318–1329.

Rivetta, C. H., Emadi, A., Williamson, G. A., Jayabalan R. & Fahimi, B. [2004] "Analysis and control of a buck DC-DC converter operating with constant power load in sea and undersea vehicles," *IEEE Transactions on Industry Applications,* **2**, 1146–1153.

Redl, R. & Novak, I. [1981] "Instabilities in current-mode controlled switching voltage regulators," *IEEE Power Electronics Specialists Conference (PESC'81)*, 17–28.

Robert R. & Robert, C. [2002] "Border collision bifurcations in a one-dimensional piecewise smooth map for a PWM current-programmed H-bridge inverter," *International Journal of Control,* **75**, **16-17**, 1356–1367.

Saublet, L., Gavagsaz-Ghoachani, R., Martin, J., Nahid-Mobarakeh, B. & Pierfederici, S. [2016] "Asymptotic stability analysis of the limit cycle of a cascaded DC–DC converter using sampled discrete-time modeling," *IEEE Transactions on Industrial Electronics*, **63**, **4**, 2477–2487.

Saublet, L., Gavagsaz-Ghoachani, R., Martin, J., Nahid-Mobarakeh, B. & Pierfederici, S. [2016] "Bifurcation analysis and stabilization of DC power systems for electrified transportation systems," *IEEE Transactions on Transportation Electrification*, **2**, **1**, 86–95.

Sulligoi, G., Bosich, D., Giadrossi, G., Zhu, L., Cupelli, M. & Monti, A. [2014] "Multiconverter medium voltage DC power systems on ships, constant power loads instability solution using linearization via state feedback control," *IEEE Transactions Smart Grids,* **5**, 2543–2552.

Tse, C. K. [2003] *Complex behavior of switching power converters,* New York: CRC Press.

Tse, C. K. [1994] "Flip bifurcation and chaos in three-state boost switching regulators," *IEEE Transactions on Circuits and Systems I: Fundamental Theory and Applications*, **41**, **1**, 16–23.

Tse, C. K. [1994] "Chaos from a buck switching regulator operating in discontinuous mode," *International Journal of Circuit Theory and Applications,* **22**, 263–278.

Tse, C. K. & Adams, K. M. [1990] "Qualitative analysis and control of a DC-to-DC boost converter operating in discontinuous mode," *IEEE Transactions on Power Electronics,* **5**, **3**, 323–330.

Tse C. K. & Li, M. [2011] "Design-oriented bifurcation analysis of power electronics systems," *International Journal of Bifurcation and Chaos,* **21**, **06**, 1523–1537.

van der Woude, J. W., de Koning, W. L. & Fuad, Y. [2002] "On the periodic behavior of PWM DC-DC converters," *IEEE Transactions on Power Electronics,* **17**, **4**, 585–595.

Wolf, D. M., Varghese M. & Sanders, S. R. [1994] "Bifurcation of power electronic circuits," *Journal of the Franklin Institute,* **331**, **6**, 957–999.

Wu, X., Tse, C. K., Wong, S. C. & Lu, J. [2006] "Fast-scale bifurcation in single-stage PFC power supplies operating with DCM boost stage and CCM forward stage," *International Journal of Circuit Theory and Applications,* **34**, 341–355.

Zadeh, M. K., Gavagsaz-Ghoachani, R., Martin, J. P., Nahid-Mobarakeh, B., Pierfederici, S. & Molinas, M. [2016] "Discrete-time modeling, stability analysis, and active stabilization of DC distribution systems with multiple constant power loads," *IEEE Transactions on Industry Applications,* **52**, **6**, 4888–4898.

Zafrany, I. & Ben-Yaakov, S. [1995] "A chaos model of subharmonic oscillations in current mode PWM boost converters," *IEEE Power Electronics Specialists Conference Rec.,* 1111–1117.

Zhang, H., Ren H. & Cui, D. [2022] "Dynamical analysis of border collision bifurcation in one-cycle controlled single-inductor dual output boost DC-DC converters," *International Journal of Bifurcation and Chaos,* **32**, **05**, 2250064.

Zhang, X., Wang, T., Bao, H., Hu, Y. & Bao, B. [2023] "Stability effect of load converter on source converter in a cascaded buck converter," *IEEE Transactions on Power Electronics,* **38**, **1**, 604–618.